Journal of Organometallic Chemistry 897 (2019) 114–119

Contents lists available at ScienceDirect

Journal of Organometallic Chemistry

journal homepage: www.elsevier.com/locate/jorganchem

A facile method to introduce iron secondary metal centers into metal–organic frameworks

Derek A. Deming [a, 1], Matthew J. Hurlock [a, 1], Xiaoyu Li [b], Kyle W. Kriegsman [a, c], Guodong Ding [a], Xiaofeng Guo [a, b, c], Qiang Zhang [a, b, *]

[a] Department of Chemistry, Washington State University, Pullman, WA, 99164, United States
[b] Materials Science and Engineering Program, Washington State University, Pullman, WA, 99164, United States
[c] Alexandra Navrotsky Institute for Experimental Thermodynamics, Washington State University, Pullman, WA, 99164, United States

ARTICLE INFO

Article history:
Received 1 April 2019
Received in revised form
28 June 2019
Accepted 29 June 2019
Available online 1 July 2019

ABSTRACT

Herein, we report the successful incorporation of iron (0) species into a 2, 2′-bipyridine functionalized metal–organic framework (MOF) (UiO-67-bpydc). Considering the limited window size of the MOF, a small molecule, iron pentacarbonyl, was used to introduce iron (0) to coordinate to the backbone of the MOF. The newly generated material contains the iron coordinated linker, $Fe(CO)_3$(bpydc), which was supported by a series of characterization techniques. DFT calculation was also used to help understand the structure of the formed complex inside the MOF. The MOF structure remained unchanged after the post-synthetic modification, and the resulted material is a great precursor to generate MOF supported catalyst.

1. Introduction

Metal–organic frameworks (MOFs) have been subjected to extensive research in recent years owing to their intrinsic porous nature and high surface area. MOFs are comprised of organic linkers and inorganic ions/clusters that can be tailored to suit a prodigious scope of applications [1–7]. The connection of the organic linkers and inorganic nodes to construct repeating, ordered structures results in permanent porosity that is advantageous for applications, such as gas adsorption and separation, sensing, and catalysis, etc. [8–16]. MOFs are more versatile compared with other porous materials, such as zeolites and mesoporous silica, owing to the fact that the organic linkers can be easily functionalized through either pre-synthesis or post-synthetic modifications [17,18]. The post-synthetic modification of MOFs is preferred over the use of pre-synthesized linkers mainly because many functional groups that cannot survive through the solvothermal synthetic condition during MOF crystal growth due to low stability [17].

Recently, the introduction of secondary metal species into MOF cavities/backbones has aroused much more interests. Through the immobilization of catalytic active sites in MOFs, various heterogeneous catalysts can be generated and used for a wide range of organic transformations. Heterogeneous catalysts offer a number of advantages such as efficient recycling, ease of separation, and stable active sites [19]. In order to construct MOFs that can tolerate the harsh catalytic reaction conditions, MOFs with high stability are usually adopted. The high stability of these MOFs is the result of strong metal–linker interactions. According to the Hard-Soft Acid-Base theory [20], MOFs formed from hard Lewis acids and hard Lewis bases are more stable than other combinations [21]. Therefore, zirconium-carboxylate based MOFs (Zr-MOFs) have been of interests for many researchers [22]. Zr-MOFs are widely studied not only because of their high thermal and chemical stability, but also because their redox innocent properties will not quench the electron transfer process in catalysis and luminescence studies [23]. In addition, Zr^{4+} prefers to coordinate to carboxylate groups instead of pyridine-based ligands. Therefore pyridine functionalized carboxylate linkers can be used to construct Zr-MOFs with accessible pyridine open pockets to coordinate to secondary metals through post-synthetic modifications [17].

We are particularly interested in developing direct methods for highly efficient introduction of secondary organometallic species into UiO-type MOFs [24]. Conventionally, metal cations are introduced into a coordination pocket, which needs to be reduced later

* Corresponding author. Department of Chemistry, Washington State University, Pullman, WA, 99164, United States.
E-mail address: q.zhang@wsu.edu (Q. Zhang).
[1] Those authors contributed equally to this work.

https://doi.org/10.1016/j.jorganchem.2019.06.037
0022-328X/

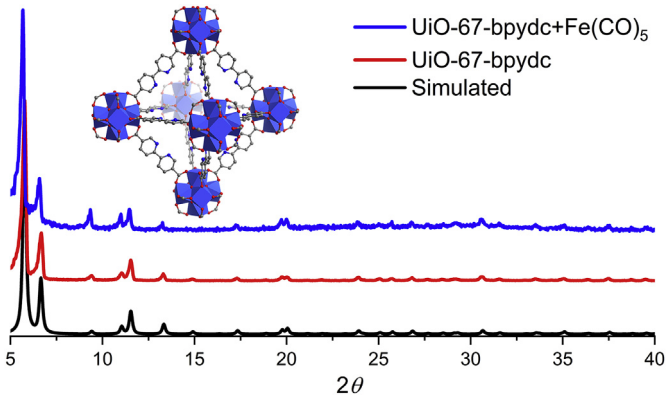

Fig. 1. The PXRD patterns from the simulated structure (black line), experimental UiO-67-bpydc (red line), and experimental UiO-67-bpydc after the addition of $Fe(CO)_5$. Inset shows the structure of UiO-67-bpydc. (For interpretation of the references to color in this figure legend, the reader is referred to the Web version of this article.)

for the use as catalysts [25]. However, the integrity of the MOF structure is compromised through this reduction process. The framework will be maintained if zero oxidation state metal species are directly incorporated. There are numerous of metal complexes with zero oxidation state metal centers, among which, transition metal carbonyl compounds are preferable candidates owing to their tunable sizes, ease of ligand exchange, and easy characterizations [26–28]. In fact, a Cr(0) carbonyl complex has been incorporated into MOFs to enhance the hydrogen storage capacity [29,30]. Herein, we report a facile strategy to incorporate an iron(0) species, $Fe(CO)_5$, into a UiO-67-bpydc (bpydc = 2,2′-bipyridine-5,5′-dicarboxylate) MOF through post-synthetic modifications. The successful introduction of iron was evidenced by the FTIR, UV–Vis, gas adsorption and EDS spectroscopies.

2. Results and discussion

The synthesis of UiO-67-bpydc was conducted with a revised procedure according to the reported method [31]. A suitable amount of $ZrOCl_2 \cdot 8H_2O$ and 2,2′-bipyridine-5,5′-dicarboxylic acid were placed in a 20 mL vial and 1 mL trifluoroacetic acid was added, the vial was then placed in a preheated oven for five days at 120 °C. White crystalline powder was obtained after washing and drying. The crystallinity and phase purity were characterized by powder X-ray diffraction (PXRD). As shown in Fig. 1, the diffraction peaks of the sample matched very-well with the PXRD pattern, simulated from the single crystal structure of UiO-67-bpydc [31].

The incorporation of $Fe(CO)_5$ was conducted in a nitrogen filled glovebox, to ensure the successful introduction of iron species, 10 fold of $Fe(CO)_5$ was used. The white powder UiO-67-bpydc, the structure is shown in Fig. 1 inset, was activated using the gas adsorption instrument before the sample was then transferred to the glovebox in a Schlenk tube. The white powder was suspended in acetonitrile and a suitable amount of $Fe(CO)_5$ was added. The reaction mixture was then stirred for 32 h at room temperature. The reaction color gradually changed from orange to dark purple after the addition of $Fe(CO)_5$. The purple powder was washed with acetonitrile several times and dried before any further characterizations. After the treatment of iron pentacarbonyl, the structure of the UiO-67-bpydc remains unchanged, which is supported by the PXRD patterns of the sample, as shown in Fig. 1 (blue line). All peaks matched very-well with the untreated UiO-67-bpydc and the simulated pattern. It is worth noting that the noise of the spectrum is due to the small sample amount. The diffraction peaks of the iron pentacarbonyl treated sample are slightly broadened compared to that of UiO-67-bpydc. This could be caused by the reduction of particle size. To prove this, SEM (Scanning Electron Microscopy) images were collected and are shown in Fig. 2. As shown in Fig. 2, the image on the left shows the morphology of UiO-67-bpydc, which consist of octahedron crystals with an averaged size of ~20 μm. However, after the treatment with $Fe(CO)_5$, the particle size decreased to less than 5 μm, which is in a great agreement with the PXRD peak broadening.

As a family of porous material, MOFs hold the record high BET (Brunauer–Emmett–Teller) surface area [32,33]. The BET surface area and the porosity of MOFs are often altered by the incorporated guest moieties. The drop in adsorption capacity, as well as the BET surface area, are usually observed. As shown in Fig. 3, the amount of nitrogen adsorbed by UiO-67-bpydc is over 600 cm^3/g, and the BET surface area is 2230 m^2/g. However, after the incorporation of $Fe(CO)_5$, the amount of nitrogen adsorbed dropped to 400 cm^3/g, and the BET surface area decreased to 1402 m^2/g. The reduced adsorption capacity and BET surface area are attributed from the added iron species that occupied partial space of the pores, which made the nitrogen hard to diffuse in. This phenomenon is very common in post-synthetic modifications of MOFs [17].

Since the sample changed from white to dark purple, we sought to measure the solid-state diffuse reflectance UV–Vis absorption spectra of the two samples to understand the photoelectronic properties. As shown in Fig. 4 (a) and (c), the UV–Vis absorption

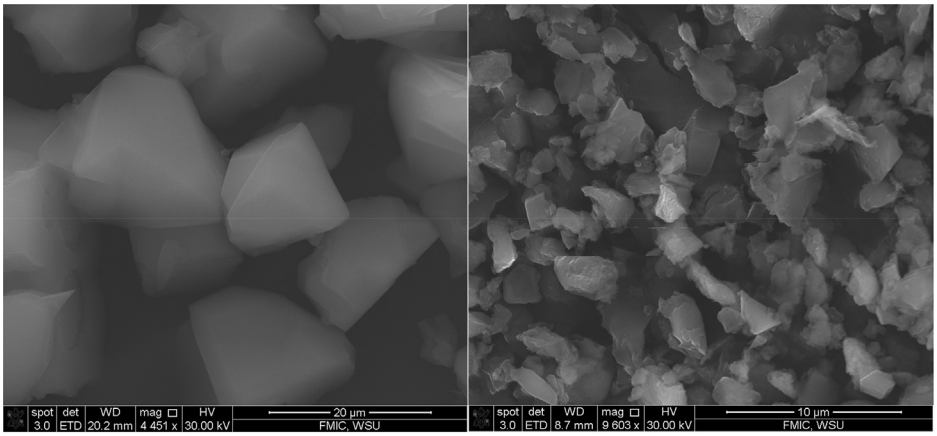

Fig. 2. SEM images of UiO-67-bpydc (left), and UiO-67-bpydc + $Fe(CO)_5$ (right).

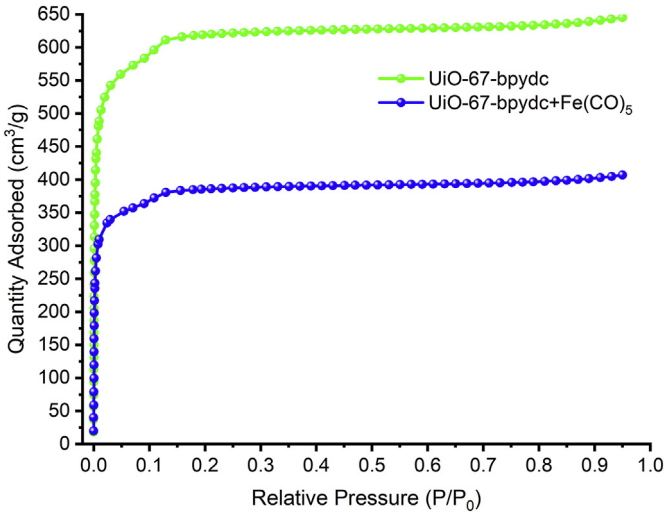

Fig. 3. The nitrogen adsorption isotherm for UiO-67-bpydc (green) and UiO-67-bpydc + $Fe(CO)_5$ (blue). (For interpretation of the references to color in this figure legend, the reader is referred to the Web version of this article.)

spectrum of UiO-67-bpydc + $Fe(CO)_5$ is very different from that of UiO-67-bpydc. The parent material, UiO-67-bpydc, possesses an absorption mainly in the ultraviolet region, whereas the iron pentacarbonyl treated shows an absorption nearly covering the entire ultraviolet and visible region. To better illustrate the differences between the two samples, Tauc plots were developed to calculate the optical band gap [34]. As demonstrated in Fig. 4 (b) and (d), the UiO-67-bpydc has an optical band gap of 3.36 eV, while the UiO-67-bpydc + $Fe(CO)_5$ shows an optical band gap of 2.38 eV. The decrease in band gap corresponds to the purple color of the UiO-67-bpdc + $Fe(CO)_5$, which is in a good agreement with the broader absorption spectrum.

The most common characterization method of transition metal carbonyl complexes is FTIR spectroscopy. The CO stretching frequencies of carbonyl complexes ranging from 1600 cm^{-1} to 2200 cm^{-1}, which can be considered as fingerprints to identify these compounds [35,36]. To evaluate the incorporation of iron carbonyl species, FTIR spectra of UiO-67-bpydc and iron carbonyl treated sample were taken using the Diffuse Reflectance Infrared Fourier Transform Spectroscopy (DRIFTS) method with the Praying Mantis accessory. As illustrated in Fig. 5, both untreated and treated samples show frequencies between 1800 cm^{-1} and 1000 cm^{-1}, which belong to C = C double bond vibrations and C–C single bond stretching. As anticipated, the UiO-67-bpydc did not show any peaks between 2100 cm^{-1} and 1800 cm^{-1}, whereas the iron

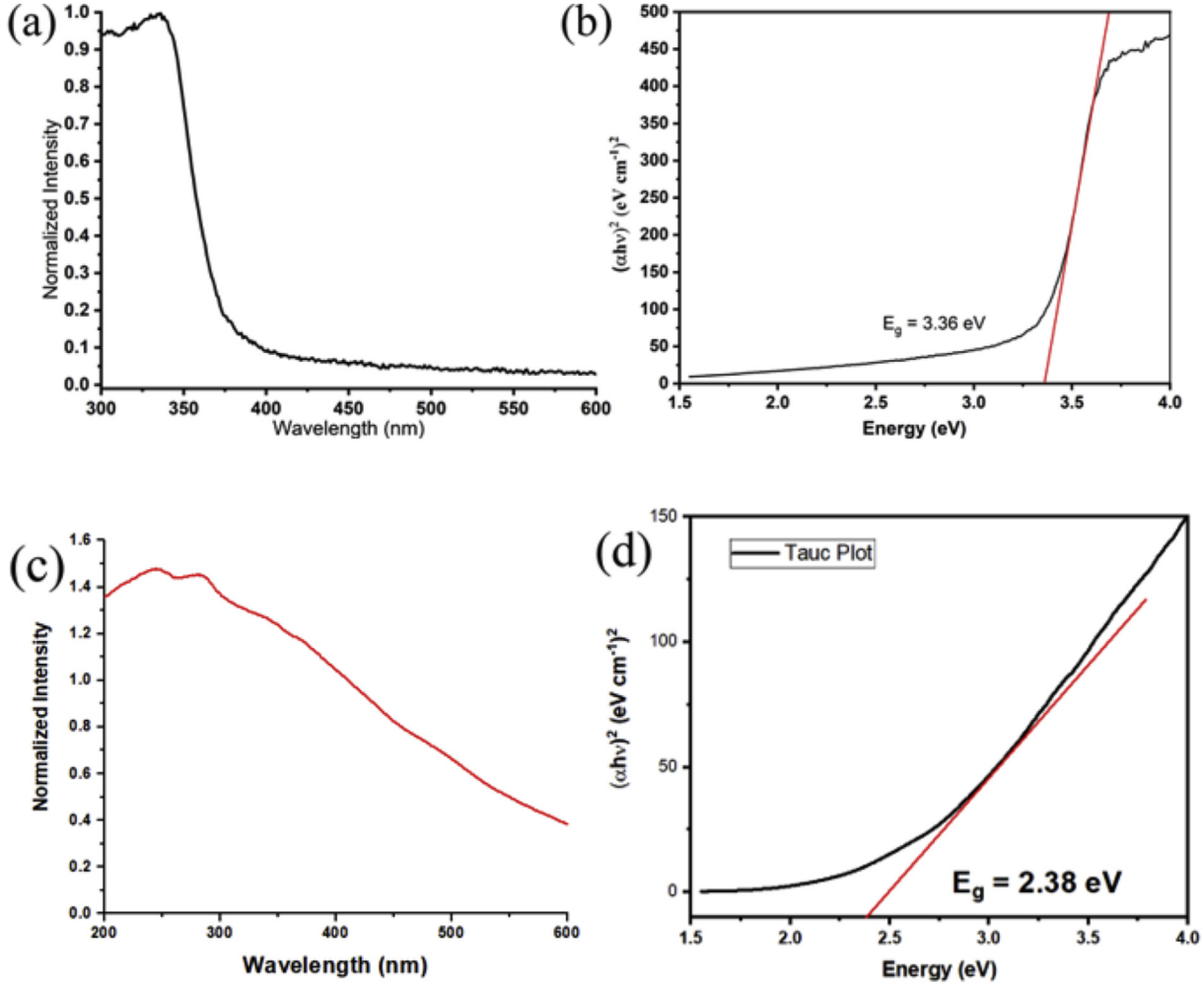

Fig. 4. The diffuse reflectance UV–Vis spectra (a) and Tauc plot (b) of UiO-67-bpydc; and diffuse reflectance UV–Vis spectra (c), and Tauc plot (d), of UiO-67-bpydc + $Fe(CO)_5$.

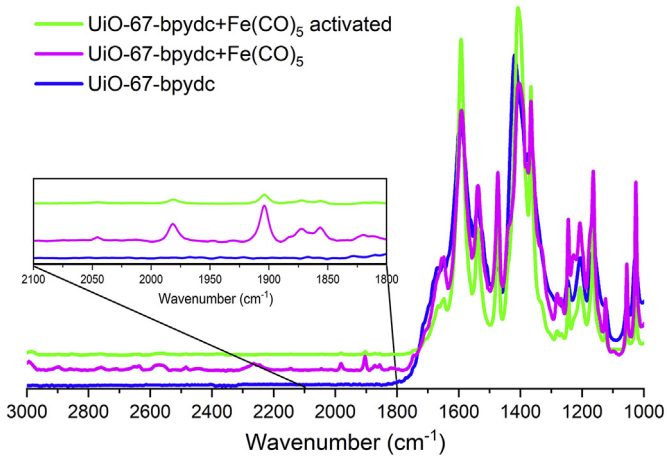

Fig. 5. The FTIR plot of UiO-67-bpydc (blue), UiO-67-bpydc + $Fe(CO)_5$ (pink) and UiO-67-bpydc + $Fe(CO)_5$ after activation (green). Inset shows spectra between 2100 cm^{-1} – 1800 cm^{-1}. (For interpretation of the references to color in this figure legend, the reader is referred to the Web version of this article.)

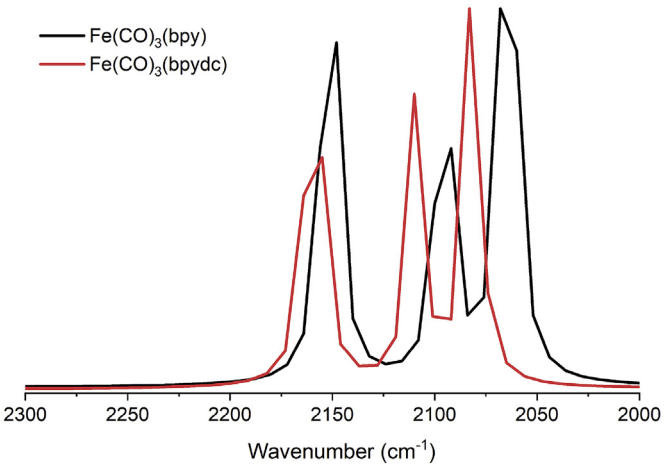

Fig. 6. DFT calculated IR spectra of $Fe(CO)_3$(bpy) (black line) and $Fe(CO)_3$(bpydc) (red line). (For interpretation of the references to color in this figure legend, the reader is referred to the Web version of this article.)

pentacarbonyl treated sample possessed several stretching peaks in this region. Since the characteristic carbonyl vibrations are around 2000 cm^{-1}, the three stretching peaks around 2000 cm^{-1} indicated that the iron pentacarbonyl treated sample contain carbonyl complexes. The peak locations are 1982 cm^{-1}, 1904 cm^{-1}, 1873 cm^{-1} and 1856 cm^{-1}, which are different from the small molecule, $Fe(CO)_3$(bpy) (bpy: 2,2′-bipyridine) (1968 cm^{-1}, 1897 cm^{-1}, 1862 cm^{-1}) [37]. The IR peaks of the material were shifted to larger wavenumbers compared to that of $Fe(CO)_3$ (bpy), which is very similar to the 1,10-phenanthroline analog $Fe(CO)_3$(phen) [37]. It is worth noting that the green spectrum in Fig. 5 represented the sample after activation. The data was collected after the nitrogen adsorption test, which was heated at 50 °C for 10 h. The decreased peak intensity was caused by partially removing of carbonyl ligands from the iron center.

Surprisingly, we were not able to find any reports about the small molecule $Fe(CO)_3$(bpydc) that in the UiO-67-bpydc + $Fe(CO)_5$ product. The attempt to synthesize the ester analog of $Fe(CO)_3$(bpydc), $Fe(CO)_3(Me_2$bpydc) Fig. S6, was not successful. The dark-colored product was very sensitive and decomposed before the purification process. To further understand the nature of the iron carbonyl compound in the MOF structure, Density Functional Theory (DFT) calculations were performed. Two molecules, $Fe(CO)_3$(bpy) and $Fe(CO)_3$(bpydc) were selected, and geometry optimization calculations were exerted, and the vibrations of the two molecules were compared. As seen in Fig. 6, the black line is the calculated FTIR spectrum for $Fe(CO)_3$(bpy), and the red line represents the $Fe(CO)_3$(bpydc) in the CO stretching region. Though the peak positions are almost 100 cm^{-1} off from the experimental data, it is not hard to see that the addition of the carboxylate groups shifted the CO vibrations to higher energy. This is in a good agreement with the experimental findings. Therefore, we believe that the carbonyl species in the iron pentacarbonyl treated UiO-67-bpydc are the $Fe(CO)_3$(bpydc) moieties. The existence of iron in the sample was also proved by the EDS spectra (energy-dispersive X-ray spectroscopy) as shown in the supporting information Fig. S5.

As mentioned above, the small molecule analog of $Fe(CO)_3$(bpydc), $Fe(CO)_3(Me_2$bpydc), is not stable, so the stability of the UiO-67-bpdc + $Fe(CO)_5$ was monitored. As shown in Fig. 5, the green profile shows the DRIFTS spectrum after activation at 50 °C for 10 h; the only change was the loss of CO stretching intensity. This is anticipated because the activation process would remove carbonyl ligands from the iron center. The color of the sample remained as purple even after days in the air at room temperature. To further evaluate the stability of the UiO-67-bpydc before and after iron incorporation, thermal gravimetric analysis (TGA) was conducted. As illustrated in Fig. 7, both samples were stable below 500 °C. UiO-67-bpydc lost 6.59% weight around 350 °C, while iron pentacarbonyl treated sample lost 7.42% weight around the same temperature. The more weight loss for the later is attributed to the loss of carbonyl ligands on the iron center.

3. Conclusions

We have demonstrated that zero oxidation state metal centers can be incorporated into MOFs by using the transition metal carbonyl complex as the precursor. This method should be a general way of introducing other metal species, the size of complexes and pore size of MOFs are the limiting factors that need to be considered when selecting the suitable pairs. The successful introduction of iron (0) species in our work was supported by FTIR, EDS mapping, and gas adsorption data. We have also performed DFT calculations to further support the formation of $Fe(CO)_3$(bpydc) analog on the MOF backbone. The use of zero oxidation state metal species in catalysis is very important in the development of highly active catalytic centers; the research in this direction is currently under investigation.

4. Experimental

4.1. General information

All commercially available chemicals were used without further purification as received unless otherwise stated. Such chemicals include $ZrOCl_2 \cdot 8H_2O$, N,N-Dimethylformamide, methanol, and trifluoroacetic acid, which were all purchased from VWR International, Sigma-Aldrich, or Bean Town Chemical. Iron pentacarbonyl was purchased from Strem Chemicals.

All MOF synthesis reactions were repeated multiple times and carried out in 20 mL glass vials in a gravity oven at 120 °C. The diffuse reflectance UV–vis and FTIR spectra were recorded on a Thermo Fisher Scientific Evolution 300 and a Nicolet™ iS10 FTIR Spectrometer with a praying mantis DRIFT accessory attached, respectively. Each spectrum was of the solid-state material with $BaSO_4$ background for the UV–Vis and KBr for the FTIR. Powder X-ray diffraction (PXRD) patterns were collected on a Rigaku Miniflex

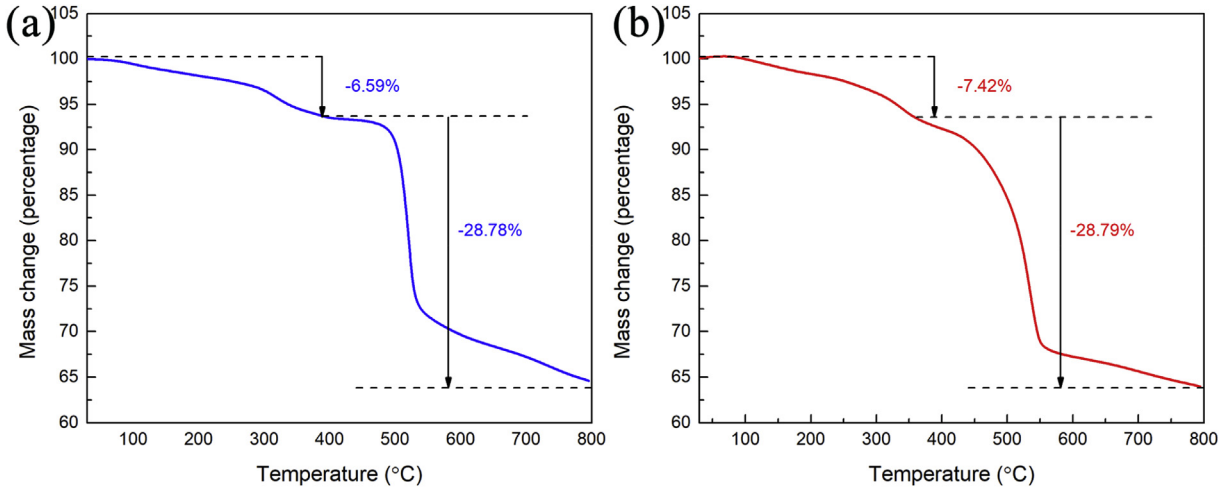

Fig. 7. Thermal gravimetric analysis (TGA) plot of UiO-67-dpydc (a), and UiO-67-dpydc + $Fe(CO)_5$ (b).

600 using Cu Kα radiation. The PXRD patterns were collected with a scan rate of 10°/min^{-1} with a step size of 0.02°. N_2 adsorption and desorption data were collected on a Micrometrics ASAP 2020 Plus accelerated surface area and porosimetry system at 77K, surface area, and pore sizes were calculated according to the nitrogen isotherms. The starting UiO-67-bpydc material was activated under vacuum at 150 °C for 12 h with the activation port equipped on ASAP 2020 Plus and analyzed for 12 h to determine the pore size and surface area. After post-metalation, UiO-67-bpydc + $Fe(CO)_5$ was activated under vacuum at 50 °C for 10 h, and analyzed for 48 h. Scanning Electron Microscopy (SEM) images were obtained by using an FEI Quanta 200 F SEM. Energy dispersive X-ray Spectroscopy (EDS) analysis was conducted by a Tescan Vega3 SEM, with 30 kV high voltage and 3.0 spot size. All powder samples were coated with 2.0 nm Pt/Pd payer before testing. Thermal gravimetric analysis (TGA) measurements were performed with a Setaram SetSYS. Suitable amount of sample was placed in an Al_2O_3 crucible without a lid and heated under nitrogen flow (20 mL/min) from 30 °C to 800 °C at a heating rate of 20 °C/min.

5. Synthesis of UiO-67-bpydc

A 5-dram vial was loaded with 40 mg of $ZrOCl_2 \cdot 8H_2O$, 20 mg of 2,2′-bipyridine-5,5′-dicarboxylic acid, 10 mL of N, N-Dimethylformamide (DMF) before being sonicated for approximately 10 min. Then 1 mL of trifluoroacetic acid was added to the vial and mixed thoroughly before it was placed in a 120 °C gravity oven for five days (~120 h). These steps were repeated for 5 vials then combined at the end of the five days into one vial after washing. The resulting solid then underwent proper filtration, washing, and soaking. Day 1 of the washing process: centrifuging at 4000 rpm for 6 min, decanting the supernatant, then rinsing with DMF and soaked in DMF overnight. Day 2 of the washing process: repeating the previous steps but rinsing with water then soaked in water overnight. Day 3 of the wash process: repeating the previous steps but rinsing with methanol and soaked in methanol overnight. The final solid was dried in a 65 °C gravity oven for 8 h before any characterizations.

6. Insertion of iron pentacarbonyl into UiO-67-bpydc

The solid UiO-67-bpydc, after activation and N_2 adsorption and desorption experiment, was used for the post-synthetic metalation. 87.4 mg of UiO-67-bpydc was stirred in 5mL acetonitrile with 1 mL of $Fe(CO)_5$ in a 5-dram vial inside a glovebox for 32 h. The color of the reaction drastically changed from dark yellow to dark purple throughout the 32 h. The reaction was stopped and washed with 10 mL of acetonitrile (3 times) and then was activated before N_2 adsorption and desorption data was collected.

DFT calculations were performed with Gaussian 09 [38] using the implemented M06–2X functional [39]. 6-31G (d,p) basis set [40] was used for the non-metal elements, and Stuttgart-Dresden (SDD) basis set was used for iron. Both structures were optimized, and vibrational spectra were calculated based on the optimized structure.

Acknowledgements

This work was supported by the Washington State University startup funds. Deming would like to thank the DOE/NE "DOE Traineeship in Nuclear and Radiochemistry Award DE-NE0008582 for the financial support. We thank Prof. Heiden and his student Ms. Brena Thompson for the help with the DFT calculations.

Appendix A. Supplementary data

Supplementary data to this article can be found online at https://doi.org/10.1016/j.jorganchem.2019.06.037.

References

[1] M.T. Huxley, C.J. Coghlan, W.M. Bloch, A. Burgun, C.J. Doonan, C.J. Sumby, Phil. Trans. Roy. Soc. A 375 (2017) 20160028.
[2] S. Kitagawa, R. Kitaura, S.-i. Noro, Angew. Chem. Int. Ed. 43 (2004) 2334–2375.
[3] O.M. Yaghi, M. O'Keeffe, N.W. Ockwig, H.K. Chae, M. Eddaoudi, J. Kim, Nature 423 (2003) 705–714.
[4] J.R. Long, O.M. Yaghi, Chem. Soc. Rev. 38 (2009) 1213–1214.
[5] H.-C. Zhou, J.R. Long, O.M. Yaghi, Chem. Rev. 112 (2012) 673–674.
[6] H.-C.J. Zhou, S. Kitagawa, Chem. Soc. Rev. 43 (2014) 5415–5418.
[7] G. Maurin, C. Serre, A. Cooper, G. Férey, Chem. Soc. Rev. 46 (2017) 3104–3107.
[8] J.D. Evans, C.J. Sumby, C.J. Doonan, Chem. Soc. Rev. 43 (2014) 5933–5951.
[9] R.J. Marshall, R.S. Forgan, Eur. J. Inorg. Chem. 2016 (2016) 4310–4331.
[10] M.P. Suh, H.J. Park, T.K. Prasad, D.-W. Lim, Chem. Rev. 112 (2012) 782–835.
[11] Y. He, W. Zhou, G. Qian, B. Chen, Chem. Soc. Rev. 43 (2014) 5657–5678.
[12] W.-Y. Gao, M. Chrzanowski, S. Ma, Chem. Soc. Rev. 43 (2014) 5841–5866.
[13] T. Zhang, W. Lin, Chem. Soc. Rev. 43 (2014) 5982–5993.
[14] J. Liu, L. Chen, H. Cui, J. Zhang, L. Zhang, C.-Y. Su, Chem. Soc. Rev. 43 (2014) 6011–6061.
[15] S.M.J. Rogge, A. Bavykina, J. Hajek, H. Garcia, A.I. Olivos-Suarez, A. Sepúlveda-Escribano, A. Vimont, G. Clet, P. Bazin, F. Kapteijn, M. Daturi, E.V. Ramos-Fernandez, F.X. Llabrés i Xamena, V. Van Speybroeck, J. Gascon, Chem. Soc. Rev. 46 (2017) 3134–3184.
[16] M.D. Allendorf, C.A. Bauer, R.K. Bhakta, R.J.T. Houk, Chem. Soc. Rev. 38 (2009)

1330–1352.
[17] S.M. Cohen, Chem. Rev. 112 (2012) 970–1000.
[18] P. Deria, J.E. Mondloch, O. Karagiaridi, W. Bury, J.T. Hupp, O.K. Farha, Chem. Soc. Rev. 43 (2014) 5896–5912.
[19] K. Sasan, Q. Lin, C. Mao, P. Feng, Chem. Commun. 50 (2014) 10390–10393.
[20] R.G. Pearson, J. Am. Chem. Soc. 85 (1963) 3533–3539.
[21] S. Yuan, L. Feng, K. Wang, J. Pang, M. Bosch, C. Lollar, Y. Sun, J. Qin, X. Yang, P. Zhang, Q. Wang, L. Zou, Y. Zhang, L. Zhang, Y. Fang, J. Li, H.-C. Zhou, Adv. Mater. 30 (2018) 1704303.
[22] Y. Bai, Y. Dou, L.-H. Xie, W. Rutledge, J.-R. Li, H.-C. Zhou, Chem. Soc. Rev. 45 (2016) 2327–2367.
[23] Q. Zhang, J. Su, D. Feng, Z. Wei, X. Zou, H.-C. Zhou, J. Am. Chem. Soc. 137 (2015) 10064–10067.
[24] J.H. Cavka, S. Jakobsen, U. Olsbye, N. Guillou, C. Lamberti, S. Bordiga, K.P. Lillerud, J. Am. Chem. Soc. 130 (2008) 13850–13851.
[25] X. Li, B. Zhang, R. Van Zeeland, L. Tang, Y. Pei, Z. Qi, T.W. Goh, L.M. Stanley, W. Huang, Catal. Lett. 148 (2018) 940–945.
[26] R.D. Adams, Y. Kan, Q. Zhang, J. Organomet. Chem. 751 (2014) 475–481.
[27] R.D. Adams, Q. Zhang, Organometallics 32 (2013) 5171–5179.
[28] R.D. Adams, Q. Zhang, X. Yang, J. Am. Chem. Soc. 133 (2011) 15950–15953.
[29] S.S. Kaye, J.R. Long, J. Am. Chem. Soc. 130 (2008) 806–807.
[30] S. Chavan, J.G. Vitillo, M.J. Uddin, F. Bonino, C. Lamberti, E. Groppo, K.-P. Lillerud, S. Bordiga, Chem. Mater. 22 (2010) 4602–4611.
[31] L. Li, S. Tang, C. Wang, X. Lv, M. Jiang, H. Wu, X. Zhao, Chem. Commun. 50 (2014) 2304–2307.
[32] O.K. Farha, I. Eryazici, N.C. Jeong, B.G. Hauser, C.E. Wilmer, A.A. Sarjeant, R.Q. Snurr, S.T. Nguyen, A.Ö. Yazaydın, J.T. Hupp, J. Am. Chem. Soc. 134 (2012) 15016–15021.
[33] S. Brunauer, P.H. Emmett, E. Teller, J. Am. Chem. Soc. 60 (1938) 309–319.
[34] J. Tauc, Mater. Res. Bull. 3 (1968) 37–46.
[35] R.D. Adams, P.J. Pellechia, M.D. Smith, Q. Zhang, J. Organomet. Chem. 706–707 (2012) 20–25.
[36] R.D. Adams, Y. Kan, Q. Zhang, M.B. Hall, E. Trufan, Organometallics 31 (2012) 50–53.
[37] M. DelaVarga, R. Costa, R. Reina, A. Núñez, M. Ángel Maestro, J. Mahía, J. Organomet. Chem. 677 (2003) 101–117.
[38] M. J. Frisch, G. W. Trucks, H. B. Schlegel, G. E. Scuseria, M. A. Robb, J. R. Cheeseman, G. Scalmani, V. Barone, G. A. Petersson, H. Nakatsuji, X. Li, M. Caricato, A. V. Marenich, J. Bloino, B. G. Janesko, R. Gomperts, B. Mennucci, H. P. Hratchian, J. V. Ortiz, A. F. Izmaylov, J. L. Sonnenberg, Williams, F. Ding, F. Lipparini, F. Egidi, J. Goings, B. Peng, A. Petrone, T. Henderson, D. Ranasinghe, V. G. Zakrzewski, J. Gao, N. Rega, G. Zheng, W. Liang, M. Hada, M. Ehara, K. Toyota, R. Fukuda, J. Hasegawa, M. Ishida, T. Nakajima, Y. Honda, O. Kitao, H. Nakai, T. Vreven, K. Throssell, J. A. Montgomery Jr., J. E. Peralta, F. Ogliaro, M. J. Bearpark, J. J. Heyd, E. N. Brothers, K. N. Kudin, V. N. Staroverov, T. A. Keith, R. Kobayashi, J. Normand, K. Raghavachari, A. P. Rendell, J. C. Burant, S. S. Iyengar, J. Tomasi, M. Cossi, J. M. Millam, M. Klene, C. Adamo, R. Cammi, J. W. Ochterski, R. L. Martin, K. Morokuma, O. Farkas, J. B. Foresman, D. J. Fox Wallingford, CT, 2016.
[39] Y. Zhao, D.G. Truhlar, J. Chem. Theory Comput. 4 (2008) 1849–1868.
[40] J.D. Dill, J.A. Pople, J. Chem. Phys. 62 (1975) 2921–2923.